Materialization of a Geometrically Frustrated Magnet in a Hybrid Coordination Framework: A Study of the Fe(II) Oxalate Fluoride Framework, $KFe(C_2O_4)F$

Katherine Tustain,[†] Lewis Farrar,[†] Wenjiao Yao,[‡] Philip Lightfoot,[‡] Ivan da Silva,[¶] Mark T. F. Telling,[¶] and Lucy Clark*,[†]

†*Department of Chemistry and Materials Innovation Factory, University of Liverpool, 51 Oxford Street, Liverpool, L7 3NY, UK*
‡*School of Chemistry, University of St Andrews, St Andrews, Fife KY16 9ST, UK*
¶*ISIS Facility, Rutherford Appleton Laboratory, Chilton, Didcot, Oxford, OX11 0QX, UK*

E-mail: lucy.clark@liverpool.ac.uk

Abstract

Here we discuss magnetic hybrid coordination frameworks in relation to the realization of new geometrically frustrated magnets. In particular, we present the nuclear and magnetic structures of one such system — the Fe^{2+}-based oxalate fluoride framework, $KFe(C_2O_4)F$ — through analysis of powder neutron diffraction and muon spectroscopy data. $KFe(C_2O_4)F$ retains an orthorhombic $Cmc2_1$ structure upon cooling to 2 K composed of quasi-one-dimensional iron fluoride chains connected into a distorted triangular network via oxalate anions. Previous magnetometry measurements of $KFe(C_2O_4)F$ indicate that it is a strongly interacting system with a Weiss constant $\theta \approx -300$ K that undergoes a magnetic ordering transition at $T_N \approx 20$ K, yielding a frustration index $f = |\theta|/T_N \approx 15$ reflective of high spin frustration. We determine the nature of this frustrated antiferromagnetic ordering below T_N, and show that the resulting magnetic structure is best described by a model in the $Cmc'2_1'$ magnetic space group.

Introduction

In crystalline solids, magnetic frustration arises through the competition of exchange interactions between magnetic moments, and is commonly observed in materials in which the geometry of the magnetic lattice affords such competing exchange. For example, materials in which antiferromagnetically coupled ions form layers of edge-sharing or corner-sharing triangles (see Figure 1) often exhibit unconventional magnetic ordering at low temperatures as a result of their ensuing geometric frustration.[1] In some cases, for instance, in the presence of quantum fluctuations, frustrated magnets may evade magnetic ordering at any measurable temperature, giving rise to the tantalising possibility of observing novel emergent phenomena in so-called spin liquid ground states.[2,3] There is a handful of canonical examples of inorganic solids based on frustrated architectures of magnetic rare-earth[4] and transition metal ions[5,6] that has been instrumental in developing our current understanding of unconventional magnetic states of matter, such as spin ices, glasses and liquids.[1] However, several crucial challenges remain in the field of highly frustrated magnetism, including understanding the
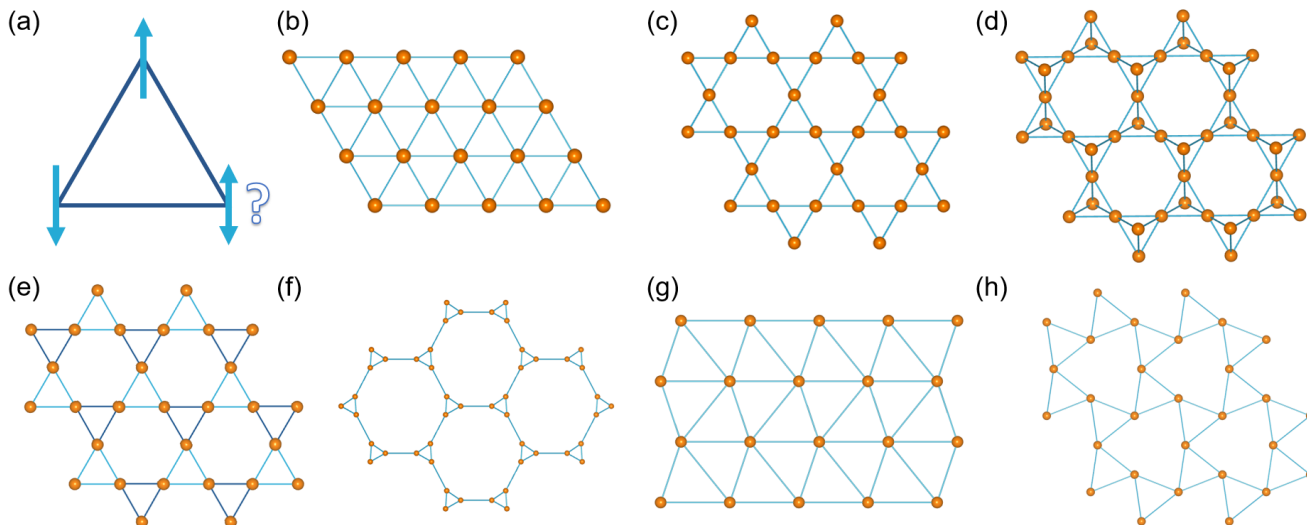
Figure 1: (a) The competing interactions of antiferromagnetically coupled spins on a triangular plaquette can result in a range of frustrated topologies that may be realized in hybrid coordination frameworks, such as (b) edge-sharing triangular[14–17] and (c) kagome[21,22] lattices. Materializations of three-dimensional frustrated lattices, such as the (d) pyrochlore[4] lattice of corner-sharing tetrahedra, are rare amongst hybrid materials, however, there are also unique examples of (e) breathing kagome[32–34] lattices, composed of alternately sized equilateral corner-sharing triangles, (f) star,[25] (g) distorted triangular[35,41] and (h) distorted kagome lattices[35,39] in hybrid coordination framework solids.

interplay between chemical and magnetic disorder,[7] revealing the properties of materials in the limit of strong spin-orbit coupling,[8] and utilizing external variables such as magnetic field and applied pressure to test the robustness of the quantum disordered phases that can arise in frustrated magnets.[9] Furthermore, there is often still a disconnect between our understanding of certain archetypal models of geometric magnetic frustration from state-of-the-art theory[10] and experiment[11] owing to the complexity of such systems. Therefore, in order to address these challenges and make new advances, different materializations of geometrically frustrated magnets are still sorely needed.

In this regard, hybrid coordination frameworks offer a versatile playground in which to explore magnetic frustration. A range of organic components are available which are able to both facilitate exchange between inorganic magnetic ions, or aid in separating magnetic components to control the overall magnetic dimensionality, and their open frameworks are often more easily tuned by modest and experimentally feasible magnetic fields and applied pressures than their purely inorganic counterparts. An early connection to the field of coordination chemistry was made by Harrison,[12] who drew inspiration from the concept of structural building units (SBUs) widely employed in the reticular synthesis of hybrid porous materials[13] for the design and synthesis of new frustrated magnets. Indeed, there are now several interesting examples of coordination frameworks where metal ions form geometrically frustrated lattices, such as the two-dimensional triangular lattice of edge-sharing triangular plaquettes.[14–18] For example, in lanthanide-based (Ln) $Ln(HCO_2)_3$, the formate ligands connect the rare-earth metal ion centres into a frustrated triangular arrangement.[17,18] Analysis of diffuse neutron scattering data suggests that these materials resemble a one-dimensional chain above their magnetic ordering transition temperatures, a feature which is thought to contribute to their functional magnetocaloric properties. Indeed, the use of organic components in hybrid magnets enables access to a range

of frustrated topologies, from one-dimensional chains [19,20] to two-dimensional corner-sharing triangular networks, referred to as kagome lattices, [21,22] and even three-dimensional structures composed of frustrated subunits [23] (see Figure 1). More complex structures such as mixed triangular-kagome and star-like lattices have been observed in Mn- and Fe-based carboxylate frameworks, respectively. [24,25] Often, the resulting topology is highly dependent on the metal centre, as has been demonstrated in $M[C(CN)_3]_2$, where M = Fe, Cr, V, which can crystallise in both triangular and kagome arrays. [22,26] Similarly, the different bridging modes of short organic linkers can influence one lattice type over another. For example, the different coordination modes of the squarate dianion $(C_4O_4)^{2-}$ have been utilised in $Co_3(OH)_2(C_4O_4)_2 \cdot xH_2O$, which displays spin-idle behaviour above its transition temperature. [16] Depending on the level of hydration, Co^{2+} ions decorate a triangular lattice but have been shown to be highly one-dimensional through inelastic neutron scattering. [27]

One of the key advantages of hybrid systems, as opposed to purely inorganic materials, is the ability to modify the organic component to control and isolate the dimensionality of the magnetic sublattice. [28] One such example is in the metal-organic framework (MOF) $[Cu_3(CO_3)_2(bpe)_3](ClO_4)_2$, where bpe is 1,2-di(4-pyridyl)ethane and Cu^{2+} ions form two-dimensional kagome layers. [29] Here, it has been demonstrated that by altering the nature of the pillaring pyridyl ligand it is possible to tune the resulting magnetic frustration. [30,31] In a similar vein, we recently developed an ionothermal synthesis strategy to uncover a family of hybrid vanadium oxyfluorides, [32] in which the inter-layer separation between slabs of breathing V^{4+}/V^{3+} kagome bi- and tri-layers can be tuned through a choice of organic cation, resulting in the realisation of a unique spin liquid ground state. [33,34]

More recently, we have continued our development of solvothermal synthesis methods to prepare a distinct family of hybrid materials containing triangular layers composed of $[Fe(C_2O_4)]_\infty$. [35] The versatile oxalate linker,

$C_2O_4{}^{2-}$, is capable of facilitating both ferromagnetic and antiferromagnetic superexchanges through magnetic centres via different bridging modes, and has been utilised extensively in the exploration of magnetic frameworks. [20,36–41] Depending on whether the oxalate linkers in our systems connect through cis or syn-$anti$ modes, or a mixture of the two, the Fe^{2+} ions may arrange in either a distorted kagome or triangular lattice, which is ultimately controlled by the inter-layer ion that links the $[Fe(C_2O_4)]_\infty$ layers together. As such, the inter-layer interactions, as well as the intra-layer topology, may be tailored by modifying the ion that separates the triangular layers. One particularly intriguing material discovered during our initial study is $KFe(C_2O_4)F$, in which the fluoride ion connects together distorted triangular $[Fe(C_2O_4)]_\infty$ layers as shown in Figure 2. From a frustrated magnetism perspective, $KFe(C_2O_4)F$ is interesting as it manifests the effects of competing exchange interactions in a number of different ways. In our earlier report of $KFe(C_2O_4)F$, [35] Curie-Weiss analysis of the magnetic susceptibility data measured above 100 K gave a Weiss constant $\theta \approx -300$ K and revealed that as the sample is cooled below 100 K a broad maximum develops in the data, indicative of the onset of short-range correlations. When the sample is further cooled below 20 K, a sharp upturn in the magnetic susceptibility suggests that $KFe(C_2O_4)F$ undergoes a transition to a long-range magnetically ordered ground state. A summary of these results are shown in Figure S1 of the Supporting Information. Given this rich temperature-dependent magnetic behaviour, further investigation of the properties of this frustrated framework material is warranted. Here we present a detailed nuclear and magnetic structural study of $KFe(C_2O_4)F$ by powder neutron diffraction to understand the nature of its frustrated magnetic ground state, complemented by muon spectroscopy measurements.
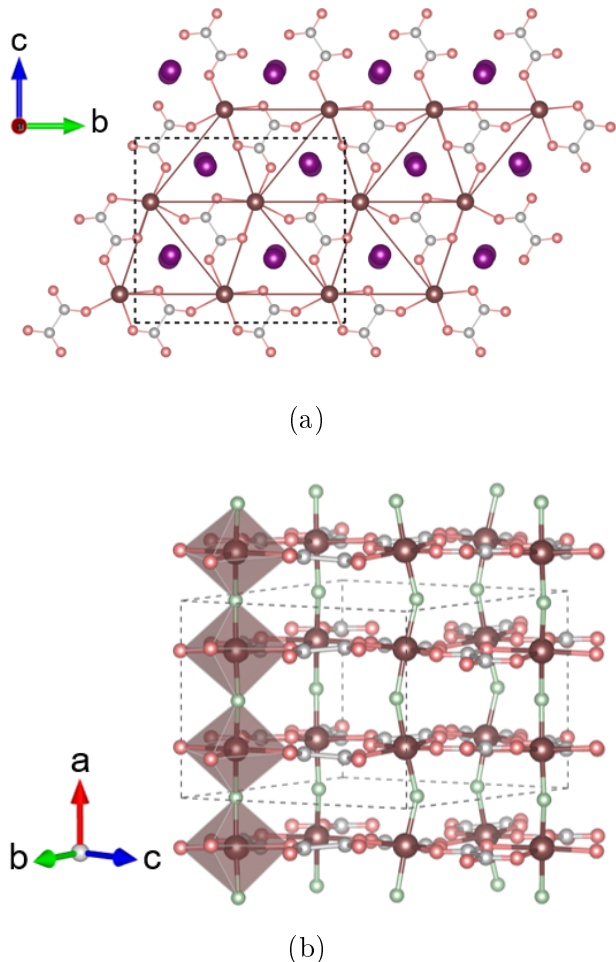
(a)

(b)

Figure 2: (a) The crystal structure of $KFe(C_2O_4)F$ viewed in the bc-plane, where Fe^{2+} ions, shown in brown, are connected via oxalate ligands and form distorted edge-sharing triangles. K^+ ions are shown in purple and occupy interlayer positions. (b) Along the a-axis, chains of corner sharing Fe^{2+} octahedra are formed via F^- linkers, shown in green. K^+ ions have been omitted here for clarity.

Experimental Section

A 1-g yellow-orange colored, polycrystalline sample of $KFe(C_2O_4)F$ was prepared via a hydrothermal synthesis method. Commercially sourced $Fe(C_2O_4)\cdot 2H_2O$, $C_2H_2O_4$, KBF_4 and K_2CO_3 were sealed in a 23-mL Teflon-lined stainless steel autoclave with distilled water in a $1:3:2:4$ molar ratio and heated at $160°C$ for 2 days. After heating, the autoclave was removed from the oven and cooled to room-temperature, with the solid product collected

by filtration and washed with distilled water and acetone. Time-of-flight powder neutron diffraction (PND) data were collected on the General Materials (GEM) diffractometer at the ISIS Neutron and Muon Facility at the Rutherford Appleton Laboratory. Data were collected on the 1-g sample at regular temperature intervals between $1.5 - 150$ K. Nuclear and magnetic structure refinements were completed using the GSAS[42,43] and FullProf[44] packages, respectively. Muon spin relaxation (μSR) measurements were performed on the same powder sample packed to a density of 170 mg/cm^2 in an aluminum sample plate in zero field (ZF) and in an applied longitudinal field (LF) of 0.01 T at temperatures between $10 - 200$ K on the MuSR spectrometer at ISIS. Supplementary data were collected on the General Purpose Surface-Muon (GPS) instrument at the Paul Scherrer Institute. Data were analyzed in the Windows Muon Data Analysis (WiMDA) program. Magnetization data as a function of field were recorded at 2 and 300 K between applied fields of $-5 - +5$ T in a Quantum Design Magnetic Properties Measurement System (MPMS).

Results and Discussion

Figure 3 shows the PND data collected on the GEM diffractometer at 150 K. Through a multibank refinement of the orthorhombic $Cmc2_1$ model shown in Table 1 — previously determined by single-crystal X-ray diffraction[35] — we confirm that this is the correct description of the structure of $KFe(C_2O_4)F$ at this temperature. All fractional coordinates were independently refined (Table 1) along with anisotropic thermal parameters (Table 2) to give an overall $R_{wp} = 2.45$ % and $\chi^2 = 1.329$. A comparison of the R_{wp} and χ^2 values obtained from Rietveld refinements using anisotropic and isotropic thermal parameters is shown in Table S1 of the Supporting Information, which indicates that the former is significant in improving the overall quality of the fit. The resulting crystal structure is shown in Figure 2 and consists of Fe^{2+} ions connected via oxalate ligands in both cis and syn-$anti$ conformations to
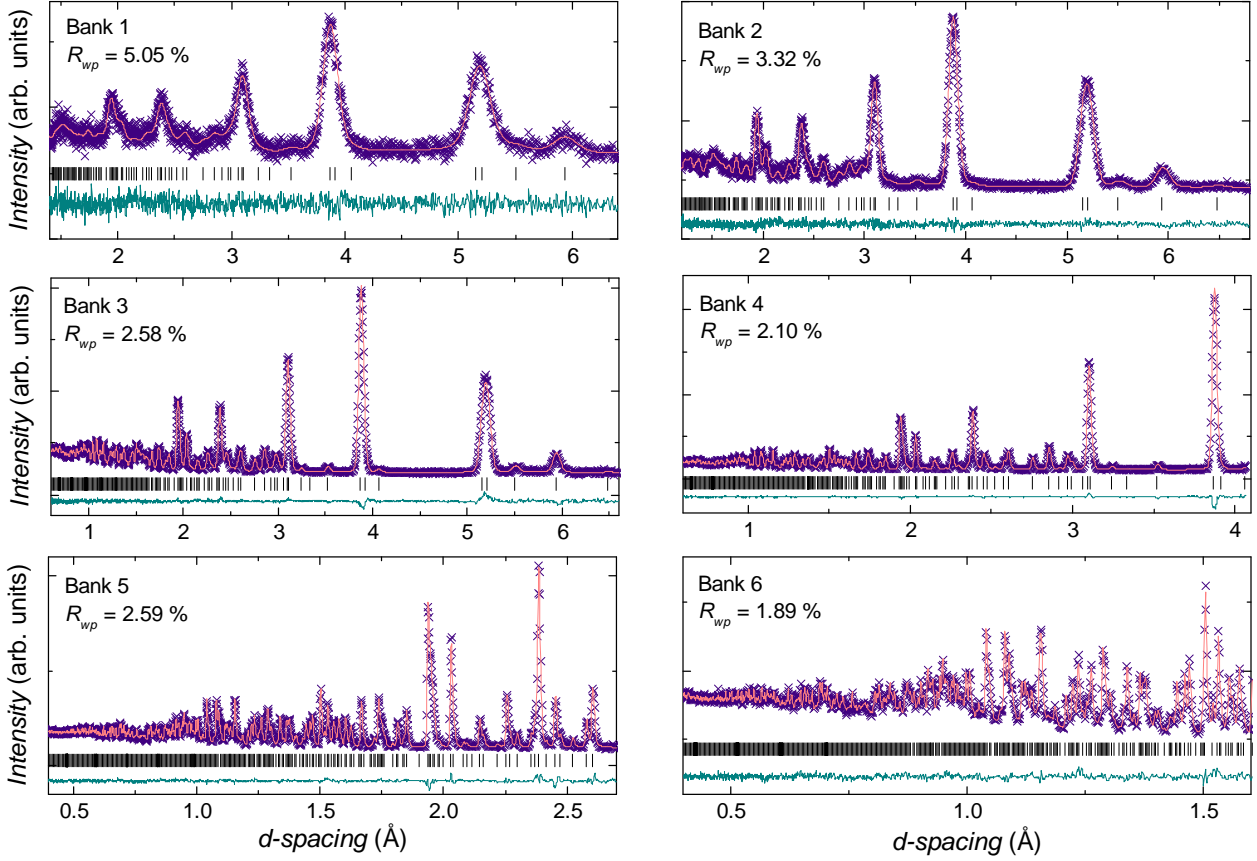
Figure 3: Rietveld refinement of the $Cmc2_1$ structural model to PND data collected on each bank of the GEM diffractometer at 150 K. Data points are shown in blue, the fitted curves are shown in pink and Bragg peak positions are represented by black tick marks.

Table 1: Nuclear structure parameters obtained from Rietveld refinement of the $Cmc2_1$ model to PND data collected at 150 K. Refined lattice parameters are $a = 7.740(1)$ Å, $b = 11.864(2)$ Å and $c = 10.409(2)$ Å (overall R_{wp}=2.45%, $\chi^2 = 1.329$).

Atom	Site	x	y	z
Fe	$8b$	0.2493(2)	0.42646(7)	0.1543(1)
K1	$4a$	0.5	0.3296(4)	0.8678(4)
K2	$4a$	0.0	0.6605(4)	0.3471(4)
O1	$8b$	0.2447(4)	0.5108(1)	0.4583(1)
O2	$8b$	0.2633(4)	0.3532(1)	0.3407(1)
O3	$8b$	0.2802(3)	0.3900(1)	0.6741(1)
O4	$8b$	0.2860(3)	0.2343(1)	0.5601(2)
C1	$8b$	0.2603(3)	0.4083(1)	0.4455(1)
C2	$8b$	0.2783(3)	0.3371(1)	0.5710(1)
F1	$4a$	0.0	0.4552(2)	0.1829(3)
F2	$4a$	0.5	0.3992(3)	0.1301(2)

form eclipsed layers of distorted edge-sharing triangles in the bc-plane. The distortion of the Fe^{2+}-based triangular network manifests as a lateral slanting of the triangular plaquettes, giving rise to three distinct in-plane nearest-neighbor Fe^{2+} exchange pathways of 5.489(2) Å and 5.932(2)Å via two Fe–O–C–O–Fe *syn-anti* bonding modes and 6.680(1) Å through a Fe–O–C–C–O–Fe *cis* linkage. Perpendicular to the triangular planes, the octahedral coordination of the Fe^{2+} ion centres is completed via F^- ion linkers, giving rise to quasi-one-dimensional Fe–F–Fe chains that run along the a-axis. The bond distances, Fe–F1 1.982(2) Å and Fe–F2 1.983(2) Å, and angles, Fe–F1–Fe 153.6(2)° and Fe–F2–Fe 156.1(2)°, within these chains imply that strong antiferromagnetic exchange correlations will dominate along the a-axis. We find that this $Cmc2_1$ model is appropriate to describe the structure of $KFe(C_2O_4)F$ to at least

Table 2: Anisotropic thermal parameters obtained from Rietveld refinement of the $Cmc2_1$ model to PND data collected at 150 K.

Atom	U_{11}	U_{22}	U_{33}	U_{aniso} (Å^2) U_{12}	U_{13}	U_{23}
Fe	0.0150(6)	0.0075(4)	0.0037(4)	0.0016(5)	0.0009(5)	0.0016(5)
K1	0.0063(11)	0.0231(14)	0.0024(12)	0.0	0.0	−0.0108(14)
K2	0.0063	0.0231	0.0024	0.0	0.0	−0.0108
O1	0.0439(5)	0.00455(27)	0.00288(26)	0.0012(6)	0.0049(6)	−0.00164(25)
O2	0.0439	0.00455	0.00288	0.0012	0.0049	−0.00164
O3	0.0439	0.00455	0.00288	0.0012	0.0049	−0.00164
O4	0.0439	0.00455	0.00288	0.0012	0.0049	−0.00164
C1	0.0253(6)	0.00417(34)	0.0052(4)	0.0004(6)	−0.0022(6)	−0.00120(29)
C2	0.0253	0.00417	0.0052	0.0004	−0.0022	−0.00120
F1	0.0042(10)	0.0513(16)	0.0120(10)	0.0	0.0	0.0053(10)
F2	0.0042	0.0513	0.0120	0.0	0.0	0.0053

1.5 K with an isotropic reduction of lattice constants and thermal parameters observed upon cooling, as shown in Figure S3 of the Supporting Information.

Figure 4(a) shows the muon decay asymmetry of positive muons implanted in KFe(C$_2$O$_4$)F in an applied longitudinal field of 0.01 T. Such a weak longitudinal field acts to decouple the muon spin from the nuclear fields within a sample, so that the muon spin directly probes the electronic magnetism arising from any unpaired electrons in a system. We find that a simple stretched exponential model is appropriate to describe the time dependence of the asymmetry, $A(t)$, data shown in Figure 4(a),

$$A(t) = A_0 \exp(-\lambda t)^\alpha + A_B \qquad (1)$$

where A_0 and A_B are the initial and background asymmetries and λ and α are the muon spin relaxation rate and stretching component, respectively. The temperature evolution of λ and α are shown together in Figure 4(b). Above 100 K, the muon asymmetry data follow a simple exponential decay with $\alpha \approx 1$, typical of the muon spin relaxation caused by electronic spin fluctuations in a paramagnetic state. However, as the sample is cooled below 100 K, α tends towards $\sim \frac{1}{3}$, indicating the onset of a spin freezing transition, or the development of a more complex distribution of internal fields at lower temperature.[45] Concomitantly, one can observe a substantial loss of initial asymmetry in the data shown in Figure 4(a) upon cooling. This implies that a significant internal field develops in KFe(C$_2$O$_4$)F, causing a rapid depolarization of the muon spin that is beyond the time resolution afforded by the pulsed muon beam on the MuSR spectrometer, which is of the order of 10 MHz. To account for this in our modelling of the data, we fixed A_0 to its full, high-temperature value, and as such, observe a critical divergence of λ below 20 K. Taken together, this suggests that the peak previously observed at the same temperature in the magnetic susceptibility marks the onset of long-range magnetic order .

To understand the nature of this long-range magnetic order, we now turn to our low-temperature PND data. As shown in Figure 5, upon cooling below 20 K we observe the evolution of additional magnetic scattering intensity in the same reflection positions as allowed nuclear Bragg peaks in the $Cmc2_1$ structure. In particular, the (111) and (110) magnetic Bragg peaks are clearly visible below 20 K in Figure 5. A set of possible magnetic space groups for the resulting $\mathbf{k} = (0, 0, 0)$ propagation vector and $Cmc2_1$ nuclear space group was generated using the BasIreps and ISODIS-

(a)

(b)

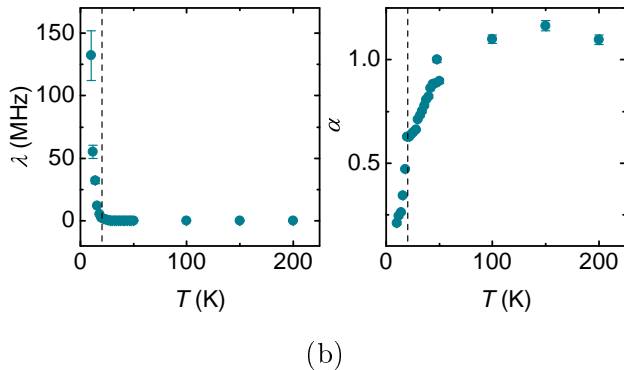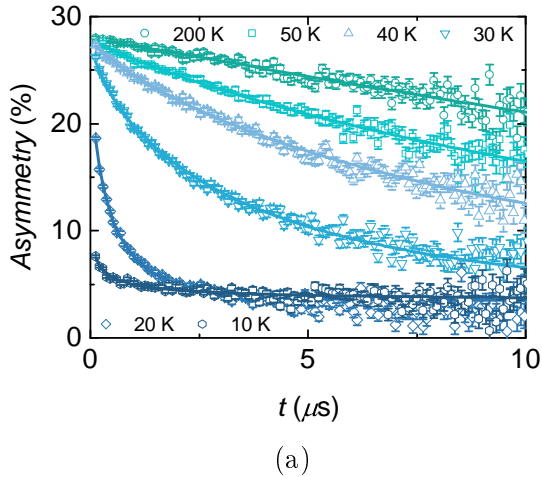Figure 4: (a) The time dependence of the muon decay asymmetry measured in $KFe(C_2O_4)F$ in an applied longitudinal field of 0.01 T between $100-200$ K on the MuSR spectrometer. Solid lines are fits to the data of the stretched exponential decay function described in the text. (b) The temperature dependence of the stretched exponential fit parameters λ, the muon spin relaxation rate, and α, the stretching component. The dotted vertical line marks the magnetic transition temperature at 20 K.

TORT[46] programs. The four possible symmetry allowed irreducible representations are $m\Gamma_1$, $m\Gamma_2$, $m\Gamma_3$, $m\Gamma_4$ in Miller-Love notation[47], which correspond to magnetic space groups $Cmc2_1$, $Cm'c'2_1$, $Cmc'2_1'$ and $Cm'c2_1'$, respectively. Full details of the magnetic structure models and a comparison of their fit to data collected at 1.5 K on GEM Bank 3 are given in the Supporting Information. We find that the $m\Gamma_3$ mode, corresponding to the $Cmc'2_1'$ magnetic space group, gives overwhelmingly the best fit to the data, which is shown in Figure 6(a). In
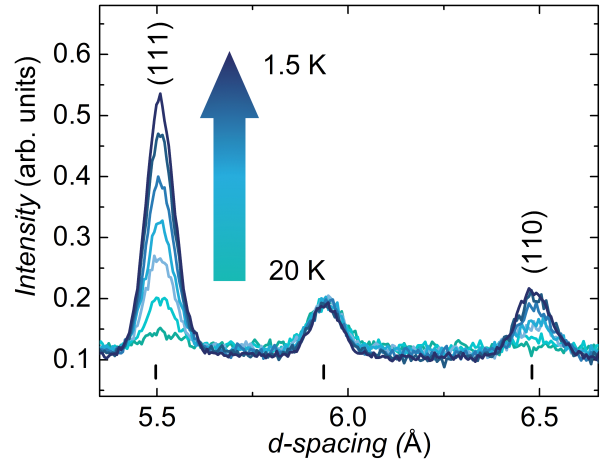

Figure 5: The evolution of the (111) and (110) magnetic Bragg peaks in the powder neutron diffraction data of $KFe(C_2O_4)F$ below 20 K.

this fit, the magnetic moment components were refined along the b- and c-axis directions, yielding $m_y = 3.41(4)$ μ_B and $m_z = 1.02(8)$ μ_B, respectively. Refinement of the magnetic moment along the a-axis did not considerably improve the fit at 1.5 K ($\chi^2 = 3.22$ compared to $\chi^2 = 3.28$ for Bank 3), and resulted in an unstable refinement at temperatures higher than 16 K. As such, the moment along the a-direction was fixed to zero, giving a total moment magnitude of $3.56(4)$ μ_B at 1.5 K, which is in keeping with the μ_{sat} value expected for an Fe^{2+} ion. Figure 6(b) shows the temperature dependence of the total ordered moment extracted from our Rietveld analysis, which can be modelled with a critical law,

$$\mu(T) = \mu_0[1 - (T/T_N)]^\beta \qquad (2)$$

giving an estimate for $T_N \approx 18.5$ K and a critical exponent $\beta \approx 0.3$ typical of three-dimensional ordering.

The resulting magnetic structure is shown in Figure 7. It can be visualized as chains of antiferromagnetically coupled Fe^{2+} moments that run along the [100] direction (Figure 7(a)) — likely mediated through the Fe–F–Fe superexchange interaction — that are arranged on the distorted triangular lattice in the bc-plane (Figure 7(b)). The moments point predominantly towards the b-axis with a small antiferromagnetic canting towards c. Such an antiferro-
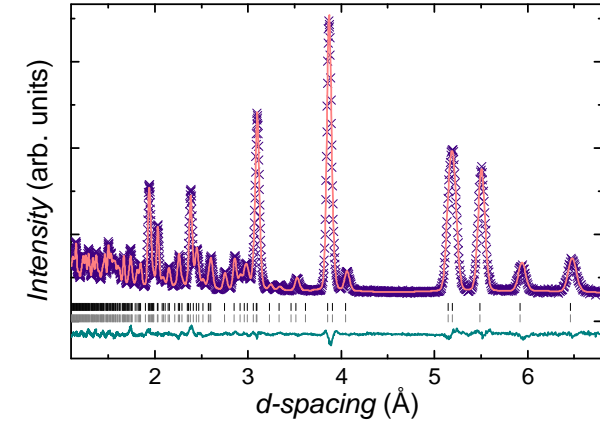
(a)
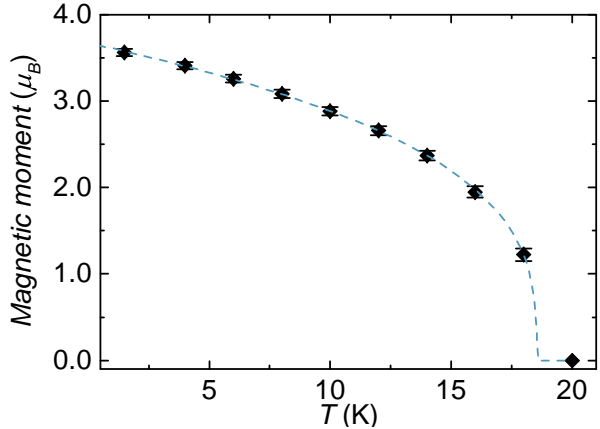
(b)

Figure 6: (a) Corefinement of the nuclear ($Cmc2_1$, top ticks) and magnetic ($Cmc'2_1'$, bottom ticks) structures to PND data collected on bank 3 of GEM at 1.5 K ($R_{wp} = 6.28\%, \chi^2 = 3.281$). (b) Temperature variation of the refined Fe^{2+} magnetic moment. The dashed blue line is a guide to the eye, showing the critical behaviour of the magnetic moment as a function of temperature.

magnetic structure is consistent with isothermal magnetization data measured below T_N, which do not indicate any significant hysteresis, but instead show a primarily linear response of a three-dimensional antiferromagnetic structure, as shown in the Supporting Information.

Conclusions

In conclusion, we have discussed the search for new paradigms in exotic magnetic ground states that emerge in geometrically frustrated mag-
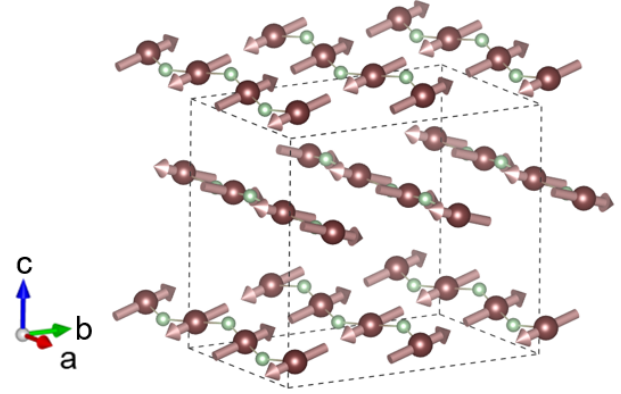
(a)
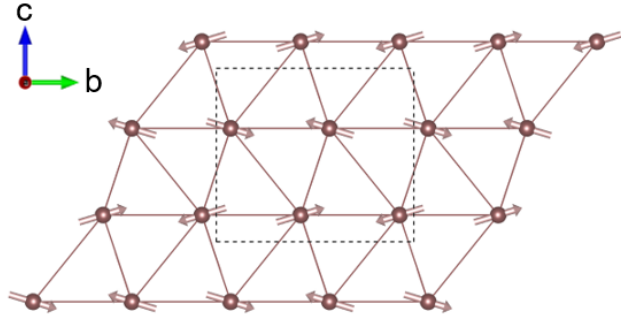
(b)

Figure 7: The magnetic structure of $KFe(C_2O_4)F$ is composed of (a) antiferromagnetically coupled chains that run along the [100] direction mediated through fluoride ion (green spheres) superexchange, which are (b) packed onto the distorted triangular layers in the bc-plane.

nets in the context of the design and synthesis of novel inorganic-organic coordination frameworks. In particular, we have examined our recent work on how one can design chemically tailorable magnetic exchange interactions in a variety of layered frustrated spin systems using different molecular building blocks. We have presented PND and μSR data for one such system, $KFe(C_2O_4)F$, which presents competing one- and two-dimensional antiferromagnetic exchange pathways. We confirm that the crystal structure of $KFe(C_2O_4)F$ is best described in the $Cmc2_1$ space group and is composed of quasi-one-dimensional Fe–F–Fe chains that run along the a-axis and form quasi-two-dimensional distorted triangular layers in the bc-plane via oxalate linkers with both cis and

syn-anti bridging modes active. Through analysis of μSR and PND data we observe critical magnetic behaviour at $T_N \approx 18.5$ K, below which the system adopts an antiferromagnetic structure described by the $Cmc'2_1'$ magnetic space group. A key feature of the magnetic structure of KFe(C_2O_4)F is the antiferromagnetic spin chains that run along the a-axis. This implies that the strongest exchange interactions in KFe(C_2O_4)F are antiferromagnetic and mediated through the fluoride anions. As such, one has to bear in mind that the reduced magnetic ordering transition temperature of KFe(C_2O_4)F in comparison to its Weiss constant may ultimately reflect the low-dimensionality of the system, rather than pronounced geometric magnetic frustration associated with the triangular $[Fe(C_2O_4)]_\infty$ layers. Therefore, insightful future studies on this system will include calculation of the various in-chain and in-plane nearest-neighbor exchange couplings, in addition to inelastic neutron scattering to determine the nature of the spin Hamiltonian.

Supporting Information Available

The following files are available free of charge.

- KFe(C_2O_4)F-Supporting-Information.pdf: this file contains supporting information regarding nuclear and magnetic structure models and refinements, supplementary μSR data, and isothermal magnetization data for KFe(C_2O_4)F at 2 K and 300 K.

- KFe(C_2O_4)F-150K.cif: this crystallographic information file contains the refined structural model for KFe(C_2O_4)F at 150 K from Rietveld analysis of PND data.

- KFe(C_2O_4)F.mcif: this magnetic crystallographic information file contains the refined magnetic structure of KFe(C_2O_4)F obtained from analysis of PND data collected at 1.5 K.

- DOI:10.5286/ISIS.E.92919513: this link provides access to raw PND data collected for KFe(C_2O_4)F on the GEM diffractometer at the ISIS Neutron and Muon Facility.

- DOI:10.5286/ISIS.E.87814807: this link provides access to raw μSR data collected for KFe(C_2O_4)F on the MuSR spectrometer at the ISIS Neutron and Muon Facility.

All other requests for data or information should be made to the corresponding author.

Acknowledgements

References

(1) Greedan, J. E. Geometrically frustrated magnetic materials. *J. Mater. Chem.* **2001**, *11*, 37–53, DOI: `10.1039/b003682j`.

(2) Balents, L. Spin liquids in frustrated magnets. *Nature* **2010**, *464*, 199–208, DOI: `doi:10.1038/nature08917`.

(3) Savary, L.; Balents, L. Quantum spin liquids: a review. *Rep. Prog. Phys.* **2016**, *80*, 016502, DOI: `10.1088/0034-4885/80/1/016502`.

(4) Bramwell, S. T.; Gingras, M. J. P. Spin Ice State in Frustrated Magnetic Pyrochlore Materials. *Science* **2001**, *294*, 1495–150, DOI: `10.1126/science.1064761`.

(5) Greedan, J. E.; Sato, M.; Yan, X.; Razavi, F. S. Spin-glass-like behavior in $Y_2Mo_2O_7$, a concentrated, crystalline system with negligible apparent disorder. *Solid State Commun.* **1986**, *59*, 895–897, DOI: `10.1016/0038-1098(86)90652-6`.

(6) Shores, M. P.; Nytko, E. A.; Bartlett, B. M.; Nocera, D. G. A Structurally Perfect $S = \frac{1}{2}$ Kagome Antiferromagnet. *J. Am. Chem. Soc.* **2005**, *127*, 13462–13463, DOI: `10.1021/ja053891p`, PMID: 16190686.

(7) Zhu, Z.; Maksimov, P. A.; White, S. R.; Chernyshev, A. L. Disorder-Induced Mimicry of a Spin Liquid in $YbMgGaO_4$. *Phys. Rev. Lett.* **2017**, *119*, 157201, DOI: `10.1103/PhysRevLett.119.157201`.

(8) Clark, L.; Sala, G.; Maharaj, D. D.; Stone, M. B.; Knight, K. S.; Telling, M. T. F.; Wang, X.; Xu, X.; Kim, J.; Li, Y.; Cheong, S.-W.; Gaulin, B. D. Two-dimensional spin liquid behaviour in the triangular-honeycomb antiferromagnet $TbInO_3$. *Nature Phys.* **2019**, DOI: `10.1038/s41567-018-0407-2`.

(9) Kozlenko, D. P.; Kusmartseva, A. F.; Lukin, E. V.; Keen, D. A.; Marshall, W. G.; de Vries, M. A.; Kamenev, K. V. From Quantum Disorder to Magnetic Order in an $S = \frac{1}{2}$ Kagome Lattice: A Structural and Magnetic Study of Herbertsmithite at High Pressure. *Phys. Rev. Lett.* **2012**, *108*, 187207, DOI: `10.1103/PhysRevLett.108.187207`.

(10) Yan, S.; Huse, D. A.; White, S. R. Spin-Liquid Ground State of the $S = \frac{1}{2}$ Kagome Heisenberg Antiferromagnet. *Science* **2012**, *332*, 1173–1176, DOI: `10.1126/science.1201080`.

(11) Han, T.-H.; Helton, J. S.; Chu, S.; Nocera, D. G.; Rodriguez-Rivera, J. A.; Broholm, C.; Lee, Y. S. Fractionalized excitations in the spin-liquid state of a kagome-lattice antiferromagnet. *Nature* **2012**, *492*, 406–410, DOI: `10.1038/nature11659`.

(12) Harrison, A. First catch your hare: the design and synthesis of frustrated magnets. *J. Phys.: Condens. Matter* **2004**, *16*, S553–S572, DOI: `10.1088/0953-8984/16/11/001`.

(13) Yaghi, O. M.; O'Keeffe, M.; Ockwig, N. W.; Chae, H. K.; Eddaoudi, M.; Kim, J. Reticular synthesis and the design of new materials. *Nature* **2003**, *423*, 705–714, DOI: `10.1038/nature01650`.

(14) Humphrey, S. M.; Wood, P. T. Multiple Areas of Magnetic Bistability in the Topological Ferrimagnet $[Co_3(NC_5H_3(CO_2)_2$-$2,5)_2(\mu_3$-$OH)_2(OH_2)_2]$. *J. Am. Chem. Soc.* **2004**, *126*, 13236–13237, DOI: `10.1021/ja0463511`.

(15) Gautier, R.; Oka, K.; Kihara, T.; Kumar, N.; Sundaresan, A.; Tokunaga, M.; Azuma, M.; Poeppelmeier, K. R. Spin Frustration from cis-Edge or -Corner Sharing Metal-Centered Octahedra. *J. Am. Chem. Soc.* **2013**, *135*, 19268–19274, DOI: `10.1021/ja409831h`.

(16) Mole, R. A.; Nadeem, M. A.; Stride, J. A.; Peterson, V. K.; Wood, P. T. Switchable Magnetism: Neutron Diffraction Studies of the Desolvated Coordination Polymer $Co_3(OH)_2(C_4O_4)_2$. *Inorg. Chem.* **2013**, *52*, 13462–13468, DOI: 10.1021/ic4018344.

(17) Saines, P. J.; Paddison, J. A. M.; Thygesen, P. M. M.; Tucker, M. G. Searching beyond Gd for magnetocaloric frameworks: magnetic properties and interactions of the $Ln(HCO_2)_3$ series. *Mater. Horiz.* **2015**, *2*, 528, DOI: 10.1039/c5mh00113g.

(18) Dixey, R. J. C.; Saines, P. J. Optimization of the Magnetocaloric Effect in Low Applied Magnetic Fields in $LnOHCO_3$ Frameworks. *Inorg. Chem.* **2018**, *57*, 12543–12551, DOI: 10.1021/acs.inorgchem.8b01549.

(19) Harcombe, D. R.; Welch, P. G.; Manuel, P.; Saines, P. J.; Goodwin, A. L. One-dimensional magnetic order in the metal-organic framework $Tb(HCOO)_3$. *Phys. Rev. B* **2016**, *94*, 174429, DOI: 10.1103/PhysRevB.94.174429.

(20) Hursthouse, M. B.; Light, M. E.; Price, D. J. One-Dimensional Magnetism in Anhydrous Iron and Cobalt Ternary Oxalates with Rare Trigonal-Prismatic Metal Coordination Environment. *Angew. Chem. Int. Ed.* **2004**, *43*, 472–475, DOI: 10.1002/anie.200352406.

(21) Nytko, E. A.; Helton, J. S.; Müller, P.; Nocera, D. G. A Structurally Perfect $S = \frac{1}{2}$ Metal-Organic Hybrid Kagome Antiferromagnet. *J. Am. Chem. Soc.* **2008**, *130*, 2922–2923, DOI: 10.1021/ja709991u.

(22) Manson, J. L.; Ressouche, E.; Miller, J. S. Spin Frustration in $M^{II}[C(CN)_3]_2$ (M = V, Cr). A Magnetism and Neutron Diffraction Study. *Inorg. Chem.* **2000**, *39*, 1135–1141, DOI: 10.1021/ic991231d.

(23) Ding, B.; Zhang, S.; Liu, Z. Y.; Yang, E. C.; Zhao, X. J. A spin-frustrated (4, 12)-connected metal-organic framework with unusual $[Co_8(\mu_4\text{-}OH)_6^{10+}]$ cubes. *Inorg. Chem. Commun.* **2017**, *83*, 27–30, DOI: 10.1016/j.inoche.2017.05.022.

(24) Wang, X.-Y.; Sevov, S. C. A Manganese Carboxylate with Geometrically Frustrated Magnetic Layers of Novel Topology. *Chem. Mater.* **2007**, *19*, 3763–3766, DOI: 10.1021/cm070713h.

(25) Zheng, Y. Z.; Tong, M. L.; Xue, W.; Zhang, W. X.; Chen, X. M.; Grandjean, F.; Long, G. J. A "Star" Antiferromagnet: A Polymeric Iron(III) Acetate That Exhibits Both Spin Frustration and Long-Range Magnetic Ordering. *Angew. Chemie - Int. Ed.* **2007**, *46*, 6076–6080, DOI: 10.1002/anie.200701954.

(26) Feyerherm, R.; Loose, A.; Landsgesell, S.; Manson, J. L. Magnetic Ordering in Iron Tricyanomethanide. *Inorg. Chem.* **2004**, *43*, 6633–6639, DOI: 10.1021/ic049423i.

(27) Mole, R. A.; Rule, K. C.; Yu, D.; Stride, J. A.; Nadeem, M. A.; Wood, P. T. Dynamics of the frustrated spin in the low dimensional magnet $Co_3(OH)_3(C_4O_4)_2$. *J. Phys.: Condens. Matter* **2016**, *28*, 126005, DOI: 10.1088/0953-8984/28/12/126005.

(28) Saines, P. J.; Bristowe, N. C. Probing magnetic interactions in metal-organic frameworks and coordination polymers microscopically. *Dalton Trans.* **2018**, *47*, 13257, DOI: 10.1039/c8dt02411a.

(29) Kanoo, P.; Madhu, C.; Mostafa, G.; Maji, T. K.; Sundaresan, A.; Pati, S. K.; Rao, C. N. R. A planar Cu^{2+} ($S = \frac{1}{2}$) kagome network pillared by 1,2-bis(4-pyridyl) ethane with interesting magnetic properties. *Dalt. Trans.* **2009**, *9226*, 5062–5064, DOI: 10.1039/b905229a.

(30) Keene, T. D.; Murphy, M. J.; Price, J. R.; Sciortino, N. F.; Southon, P. D.; Kepert, C. J. Multifunctional MOFs through CO_2 fixation: a metamagnetic

kagome lattice with uniaxial zero thermal expansion and reversible guest sorption. *Dalt. Trans.* **2014**, *43*, 14766–14771, DOI: `10.1039/C4DT02205J`.

(31) Ajeesh, M. O.; Yogi, A.; Padmanabhan, M.; Nath, R. Tuning of magnetic frustration in $S = \frac{1}{2}$ Kagome lattices $[Cu_3(CO_3)_2(bpe)_3](ClO_4)_2]_n$ and $[Cu_3(CO_3)_2(bpy)_3(ClO_4)]_{2n}$ through rigid and flexible ligands. *Solid State Commun.* **2015**, *207*, 16–20, DOI: `10.1016/j.ssc.2015.01.018`.

(32) Clark, L.; Aidoudi, F. H.; Black, C.; Arachchige, K. S. A.; Slawin, A. M. Z.; Morris, R. E.; Lightfoot, P. Extending the Family of V^{4+} $S = \frac{1}{2}$ Kagome Antiferromagnets. *Angew. Chem. Int. Ed.* **2015**, *54*, 15457–15461, DOI: `10.1002/anie.201506869`.

(33) Clark, L.; Orain, J. C.; Bert, F.; De Vries, M. A.; Aidoudi, F. H.; Morris, R. E.; Lightfoot, P.; Lord, J. S.; Telling, M. T. F.; Bonville, P.; Attfield, J. P.; Mendels, P.; Harrison, A. Gapless Spin Liquid Ground State in the $S = \frac{1}{2}$ Vanadium Oxyfluoride Kagome Antiferromagnet $[NH_4][C_7H_{14}N][V_7O_6F_{18}]$. *Phys. Rev. Lett.* **2013**, *110*, 207208, DOI: `10.1103/PhysRevLett.110.207208`.

(34) Orain, J.-C.; Bernu, B.; Mendels, P.; Clark, L.; Aidoudi, F. H.; Lightfoot, P.; Morris, R. E.; Bert, F. Nature of the Spin Liquid Ground State in a Breathing Kagome Compound Studied by NMR and Series Expansion. *Phys. Rev. Lett.* **2017**, *118*, 237203, DOI: `10.1103/PhysRevLett.118.237203`.

(35) Yao, W.; Clark, L.; Xia, M.; Li, T.; Lee, S. L.; Lightfoot, P. Diverse Family of Layered Frustrated Magnets with Tailorable Interlayer Interactions. *Chem. Mater.* **2017**, *29*, 6616–6620.

(36) Watts, I. D.; Carling, S. G.; Day, P. Site dilution of two-dimensional honeycomb molecular ferrimagnets $AFe^{II}Fe^{III}(C_2O_4)_3$

$(A = (n\text{-}C_4H_9)N, P(C_6H_5)_4)$. *Phys. Chem. Chem. Phys.* **2001**, *3*, 4418–4422, DOI: `10.1039/b103999g`.

(37) Andrés, R.; Brissard, M.; Gruselle, M.; Train, C.; Vaissermann, J.; Malézieux, B.; Jamet, J.-P.; Verdaguer, M. Rational Design of Three-Dimensional (3D) Optically Active Molecule-Based Magnets: Synthesis, Structure, Optical and Magnetic Properties of $[Ru(bpy)_3]^{2+}$, ClO_4^-, $[Mn^{II}Cr^{III}(ox)_3]^-_n$ and $[Ru(bpy)_2ppy]^+$. *Inorg. Chem.* **2001**, *40*, 4633–4640, DOI: `10.1021/ic010363f`.

(38) Price, D. J.; Powell, A. K.; Wood, P. T. A new series of layered transition metal oxalates: hydrothermal synthesis, structural and magnetic studies. *Dalt. Trans.* **2003**, 2478–2482, DOI: `10.1039/b301658g`.

(39) Li, J.-H.; Liu, H.; Wei, L.; Wang, G.-M. Two novel Fe II-oxalate architectures: Solvent-free synthesis, structures, thermal and magnetic studies. *Solid State Sci.* **2015**, *48*, 225–229, DOI: `10.1016/j.solidstatesciences.2015.08.017`.

(40) Rousse, G.; Rodríguez-Carvajal, J. Oxalate-mediated long-range antiferromagnetism order in $Fe_2(C_2O_4)_3 \cdot 4H_2O$. *Dalt. Trans.* **2016**, *45*, 14311–14319, DOI: `10.1039/c6dt02740g`.

(41) Yao, W.; Sougrati, M.-T.; Hoang, K.; Hui, J.; Lightfoot, P.; Armstrong, A. R. $Na_2Fe(C_2O_4)F_2$: A New Iron-Based Polyoxyanion Cathode for Li/Na Ion Batteries. *Chem.* **2017**, *29*, 2167–2172, DOI: `10.1021/acs.chemmater.6b04859`.

(42) Larson, A. C.; von Dreele, R. B. General Structure Analysis System (GSAS). *Los Alamos National Laboratory Report LAUR 86-748* **2000**,

(43) Toby, B. H. EXPGUI, a graphical user interface for GSAS. *J. Appl. Cryst.* **2001**, *34*, 210–213, DOI: `10.1107/S0021889801002242`.

(44) Rodriguez-Carvajal, J. Recent advances in magnetic structure determination by neutron powder diffraction. *Physica B* **1993**, *192*, 55–69, DOI: `10.1016/0921-4526(93)90108-I`.

(45) Stewart, J. R.; Cywinski, R. μSR evidence for the spin-liquid–to–spin-glass transition in $\beta - \mathrm{Mn}_{1-x}\mathrm{Al}_x$. *Phys. Rev. B* **1999**, *59*, 4305–4313, DOI: `10.1103/PhysRevB.59.4305`.

(46) Campbell, B. J.; Stokes, H. T.; Tanner, D. E.; Hatch, D. M. ISODISPLACE computer programs. *J. Appl. Cryst.* **2006**, *39*, 607–614, DOI: `10.1107/S0021889806014075`.

(47) Miller, S. C.; Love, W. F. *Tables of irreducible representations of space groups and co-representations of magnetic space groups*; Pruett, Boulder, 1967.

TOC Synopsis:

We present powder neutron diffraction and muon spectroscopy data for the Fe(II)-based oxalate fluoride hybrid framework solid, $KFe(C_2O_4)F$. We show that its structure is composed of distorted triangular planes of Fe(II) moments connected via fluoride anions that mediate strong antiferromagnetic exchange interactions. Below T_N, our data and analysis reveal that a frustrated canted antiferromagnetic ordering of spins emerges.